# EXPERIMENTAL VALIDATION OF ROTOR BROADBAND NOISE MODELS FOR AAM IN URBAN ENVIRONMENT

R. Habing*, P. Admiraal*, R. Bakker*, H. Dekker*, K. Knepper*
*Royal Netherlands Aerospace Centre (NLR), The Netherlands

**Abstract**

New technologies are paving the way for Advanced Air Mobility (AAM) like Urban Air Mobility (UAM) and Unmanned Aerial Vehicles (UAV). Numerous of such systems are being developed and a common architecture is electrically driven multi-rotors for thrust generation. Besides thrust, rotors also generate noise, causing annoyance for people in and around the AAM. Predicting this noise is therefore important for policy makers and developers of AAM. This paper describes the experimental validation of a recently developed noise prediction tool for AAM in urban environments, yielding a Virtual Reality environment. The focus is on rotor broadband noise, as its contribution to human perception is currently not well understood. First an overview of the considered semi-empirical broadband noise models is presented. Then a first validation step is described for an isolated single drone rotor in a wind tunnel test setup. Secondly, validation of a full multi-rotor drone flyover field test is described. Spectrograms show in general an underprediction for all noise components. Low-frequency range predictions show the improvement potential by including turbulence ingestion. The need for further research to improve the middle frequency range prediction is discussed.

## 1. NOTATION

Acronyms:

| | |
|---|---|
| AAM | Advanced Air Mobility |
| AWT | NLR's Anechoic Wind Tunnel |
| BPF | Blade Passing Frequency |
| BPM | Brooks-Pope-Marcolini model |
| eVTOL | Electric Vertical Take-Off and Landing |
| GL | Gill-Lee model |
| Pegg | Pegg model |
| ROLLNAX | Rotating Lifting Line Non-Axial |
| SPL | Sound Pressure Level |
| TI | Turbulence Ingestion model |
| UAM | Urban Air Mobility |
| UAV | Unmanned Aerial Vehicle |
| WT | Wind Tunnel |

## 2. INTRODUCTION

New technologies are paving the way for Advanced Air Mobility (AAM) like Urban Air Mobility (UAM) and Unmanned Aerial Vehicles (UAV). Numerous of such systems are being developed and a common architecture is electrically driven multi-rotors for thrust generation. Besides thrust, rotors also generate noise, causing annoyance for people in and around the AAM. Predicting this noise is therefore important for policy makers and developers of AAM.

Greenwood et. al [1] presented an overview of the challenges and opportunities for low-noise electric aircraft, with focus on eVTOL noise source mechanisms and prediction. They show an overview of the taxonomy of rotor noise sources, which is based on the work of Brooks and Schlinker [2]. UAM and UAV can be classified by their rotor scales with relatively low to medium i) chord Reynolds number and ii) tip Mach number, contrary to e.g. helicopters and conventional propeller aircraft (high tip Mach number) or wind turbines (high chord Reynolds number).

For UAM and UAV it therefore can be expected that besides rotor tonal noise, also rotor broadband noise plays a significant role in the noise generation, but also in the noise propagation and eventually human noise annoyance perception in urban environment. A rotor broadband noise spectrum typically covers a relative high-frequency range, which noise levels could exceed background noise [17].

This paper describes the experimental validation of a recently developed noise prediction tool for AAM in urban environments, yielding a Virtual Reality environment [3]. The focus is on multi-rotor broadband noise as its contribution to human perception is currently not well understood [22]. First an overview of the considered semi-empirical broadband noise models is presented. Then a first validation step is described for an isolated single drone rotor in a wind tunnel test setup. Secondly, validation of a full multi-rotor drone flyover field test is described. The noise predictions are compared to experimental data for hover, low-speed flyover and high-speed flyover conditions.

## 3. NOISE SOURCE MODELLING

### 3.1. Prediction tool

Figure *1* shows an overview of the recently developed prediction tool [3]. Starting from known blade planform geometry and flight conditions (in a wind tunnel the free-stream flow direction resembles the opposite flight direction), the blade sectional aerodynamic coefficients are obtained from either open source tool XOIL [4] or in-house URANS simulations. The commercially available tool FLIGHTLAB [5] then simulates the rotor unsteady aerodynamic loads (time domain), by including rotor-to-rotor interactions and airframe-to-rotor interactions through a Viscous Vortex Particle Method (VVPM) solver. NLR's rotating lifting line tool adapted for non-axial flow ROLLNAX [3,6,7] computes the tonal noise. Rotor broadband noise is predicted by implemented semi-empirical models (see section 3.2).

Finally, hemispheres spectra in 1/3-octave bands represent the noise source sound pressure level scaled to a reference distance and directivity, see Figure 2. Recently NLR's low-fidelity noise prediction tool for AAM in urban environment has been presented as full tool chain without validation [3]. The prediction tool has three parts, i.e. 1) noise source modelling, 2) noise propagation modelling, and 3) noise annoyance perception. The present paper is related to the toolchain part of noise source modelling.

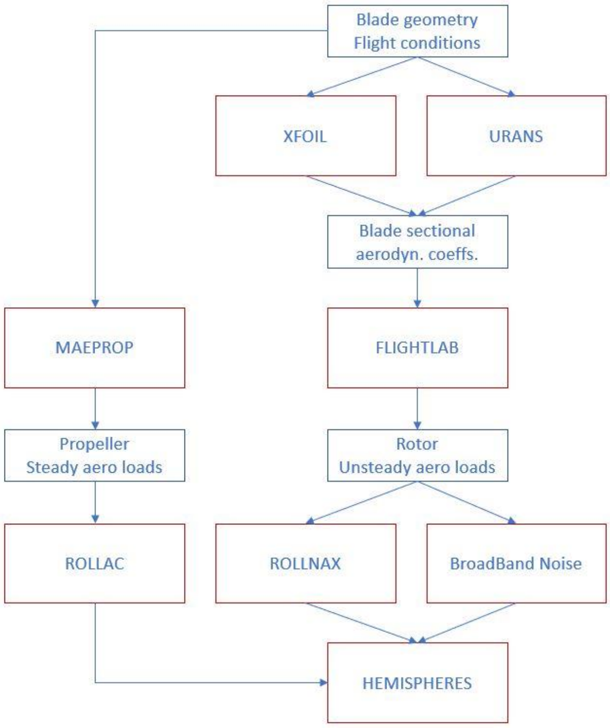


Figure 1: Flow chart of noise source prediction tool.

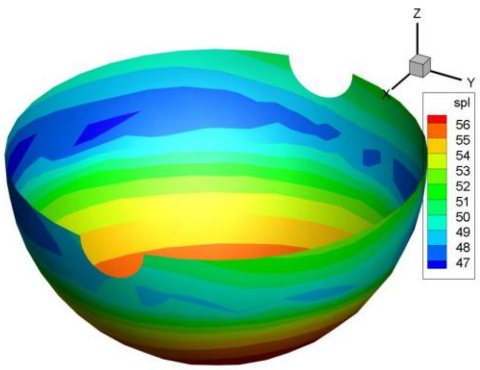


Figure 2: Example of a hemisphere as broadband noise source [3].

### 3.2. Rotor broadband noise models

Following the taxonomy of rotor noise sources of Greenwood et al. [1], non-deterministic loading noise can be divided into narrowband and broadband sources. Non-deterministic narrowband loading noise (or narrowband random noise) is generally related to turbulence ingestion of atmospheric or a turbulent wake into the rotor or propeller. As the rotor "chops" several times through a turbulent eddy, the result is a narrowband random noise source, that is characterized as broad spectral peaks around the blade passage frequency and its harmonics. Broadband noise is characterized by a broad noise spectrum caused by unsteady turbulent loading due to blade-wake interaction, turbulence in the boundary layer (for blade self-noise), and turbulence ingestion [1].

Rotor broadband noise is predicted by implemented semi-empirical models and have their benefit in reduced computational costs. The following methods have been implemented, referred to as: BPM [8], Pegg [10], GL [11] and recently TI [12].

### 3.2.1 Pegg model

The Pegg model [10] is based upon the assumption that broadband noise from a surface in a moving flow can be described by at least three mechanisms which generate random, fluctuating forces. These mechanisms include the surface pressure field which arises from a turbulent boundary layer (Boundary Layer Noise), the force fluctuations which can arise if the surface is moving in an initially-turbulent flow (Inflow Turbulence Noise) and a third, fluctuating force that results from shed vorticity (Vortex Noise). This approach avoids the treatment of noise sources as compact, instead assuming that the plate (rotor blade) dimension is of the order of the acoustic wavelength.

Pegg's model is relative simple to implement, computationally very efficient and reasonably accurate for low to moderate advance ratios. The method is fundamentally based on helicopter rotor acoustics. It generates a 1/3 octave band spectrum and does not provide any measure of how various mechanisms contribute independently.

### 3.2.2 BPM model

The model of Brooks, Pope and Marcolini (BPM) [8] was developed to predict self-generated noise of an airfoil encountering smooth airflow. BPM models five self-noise mechanisms due to boundary-layer phenomena: 1) boundary-layer turbulence passing over the trailing edge, 2) separated-boundary layer and stalled airfoil flow, 3) vortex shedding from laminar-boundary-layer instabilities, 4) vortex shedding from blunt trailing edges, and 5) turbulent vortex flow that exists near the tips of lifting blades. This method is based upon noise results from experimental tests of seven NACA0012 airfoil blade sections with chord lengths ranging from 2.5 to 61 cm which were performed at wind tunnel speeds up to Mach 0.21 and angles of attack from 0 to 25.2 deg. It is noted that these tests considered steady inflow and fixed (i.e. non-rotating) airfoils.

While significantly more complex than Pegg's model, the BPM model generates noise predictions for each noise mechanism separately. The noise levels predicted in BPM's model are dependent on the Strouhal number which is defined in various forms depending on the specific noise mechanism. This dependence on frequency requires an additional step in the prediction process. A frequency correction factor must be applied to account for the perceived shift in frequency that is produced when the source and observer and are in motion, commonly known as the Doppler effect. The BPM model is also included in NLR's aircraft noise prediction tool ENOISE as wing trailing edge noise source [9]. NLR's multi-rotor noise prediction tool has been modified to allow reading of specific boundary layer input, generated by e.g. XFOIL. It is stated that blade specific boundary layer parameters obtained with XFOIL did not improve the BPM predictions of present test cases [21]. Further research is needed to understand this improvement potential and is beyond the scope of the present paper.

### 3.2.3 TI model

As the BPM model considers trailing edge (TE) noise, the broadband noise prediction could be extended by considering turbulence ingestion as well. The rotor turbulence ingestion (TI) model is based on a wind turbine turbulent inflow noise prediction model [12]. Recently, TI noise and TE noise spectra have been separately predicted in a benchmark study for wind turbine noise [18]. The third-octave band SPL spectrum is taken from a high-frequency asymptote (matching the von Kármán spectrum to the Kolmogorov turbulence spectrum) typical for wind turbines [12]. The atmospheric turbulence dissipation rate can be obtained from measurements and is a function of (aircraft) height and wind speed. The directivity function from the BPM model implementation can be used, assuming the observer – rotor distance is much larger than the blade chord, and the noise radiation pattern is not directed towards leading edge (LE) but towards TE (i.e. mirrored).

### 3.2.4 GL model

Recently, Gill and Lee published a novel empirical model for rotor broadband noise [11], which we will refer to as the GL model. A dataset comprising hundreds of noise recordings from a variety of rotors was utilized (small drones, medium-size propellers and large helicopter rotors). An evolutionary machine learning algorithm was employed to develop a new broadband noise spectrum model. The blade tip Mach number distribution shows a normal pattern in the range 0.08 – 0.67. However, the dataset does not encompass scenarios with low tip speeds and low blade loadings, as well as high tip speeds with low blade loading. The GL model is relatively simple to implement and generates a 1/3 octave band SPL spectrum.

## 4. WIND TUNNEL TESTS OF SINGLE ROTOR

### 4.1. Test and measurement setup

In order to generate an experimental database to be used for single rotor noise validation purposes, two test campaigns have been performed. Both tests have been performed in NLR's anechoic wind tunnel facility AWT. The AWT is a low cost, easy access tunnel used for i) research (low TRL), ii) development of measurement techniques, iii) concept testing.

The first test considered a commercially available drone rotor (DJI 2170R) under various representative test conditions (hover, flyover speed 5, 10 and 18 m/s, vertical take-off and landing; various rotor axis – flight direction angles by control of a turntable and various RPM to simulate consistent flight; rotor tip Mach number range was approx. 0.19 - 0.33). A high-power electric motor was used (Hacker Q80-6L V2) to avoid heat issues at continuous high power runs. A 6-component balance was used to measure the steady loads. Care should be taken in limiting rotor dimensions to avoid WT shear layer ingestion and WT nozzle – rotor streamtube interference. The noise measurements were conducted with a microphone line array (50 – 140 deg), see Figure 3 - Figure 4. Both the test hall and model support was acoustically treated during noise measurements.

The second test was a repeat of the hover conditions for the same drone propeller, but with original electric motor (DJI 6010), limited to 3 emission angles (35, 90 and 145 deg) with different microphone positions. The blade geometry was optically scanned at 10 sections to feed the prediction tool.

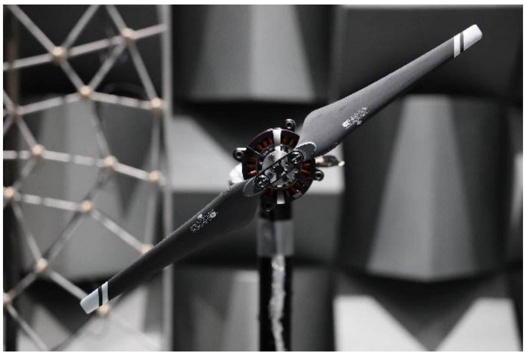

Figure 3: Single rotor test setup: front view picture.

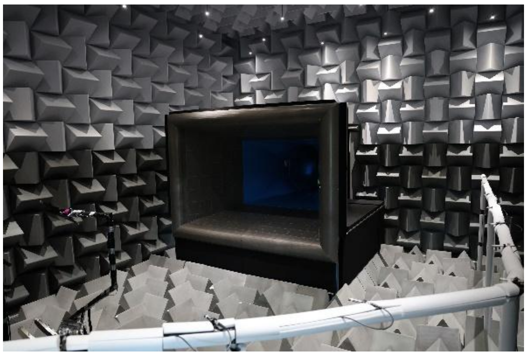

Figure 4: Microphone line array in open test section of NLR's AWT facility

### 4.2. Validation results

In order to reveal detailed experimental noise data, the SPL spectra are processed as narrowband with a resolution of 10 Hz. For comparison reasons the measured SPL is corrected to a reference distance of 5m for all microphone positions. It is noted that the microphones are in most cases in the tonal farfield, with exceptions for some cases of the first BPF. However, the present paper focuses on rotor broadband noise which is considered to be of random noise type (in higher frequency range). Furthermore, based on initial assessments no corrections for atmospheric damping effects have been applied. Predictions from the broadband models result in 1/3 octave band spectra. In order to allow comparisons with test data, the predicted SPL are corrected to identical narrowband frequency resolution.

Figure 5 shows a comparison of the rotor broadband noise at 35 deg observer angle. The test data shows peaks over a broad frequency range. These have been identified as engine orders, with dominant peaks at even engine orders (i.e. BPFs). Comparison with motor-only and background noise spectra showed that sufficient signal-to-noise ratio is obtained in a broad frequency range. Figure 5 shows that the BPM model significantly overpredicts the peak frequency and slightly underpredicts the peak level. Simulating a tripped condition shows improvement in peak frequency but does not change the spectral slopes. Furthermore, Pegg's model significantly underpredicts the peak frequency, overpredicts the peak level but has similar negative slope. Finally, the GL model does not seem to agree at all. No implementation errors were found. Further analysis showed that the GL model is not suited for the hemisphere approach, as it does not have a far-field solution. Predicting the SPL spectrum directly for the microphone locations did improve the agreement with the measurement data. This might be related to the directivity model setting a constraint for the relative observation distance.

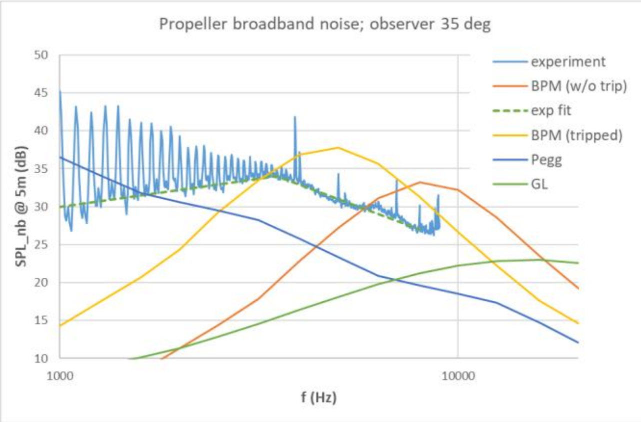


Figure 5: Comparison broadband noise prediction vs. measurement for single rotor hover condition.

### 4.3. Motor noise

AAM propeller or rotor testing in a WT requires an electric motor drive which in general could be non-representative. This leads to parasitic noise sources that need to be understood to allow analysis of especially high-frequency broadband noise.

In order to start investigating motor noise, for the first test campaign a dedicated magnetic brake was realized, see Figure 6. It consists of i) a rotatable shaft mounted aluminum disk, ii) a housing including 20 strong magnetic disks, distributed in circumferential direction, an iii) a traverse system for variation of axial distance between alu disk and magnetic front plane. This setup is limited to testing for hover conditions (i.e. no wind) and small directivity ranges.

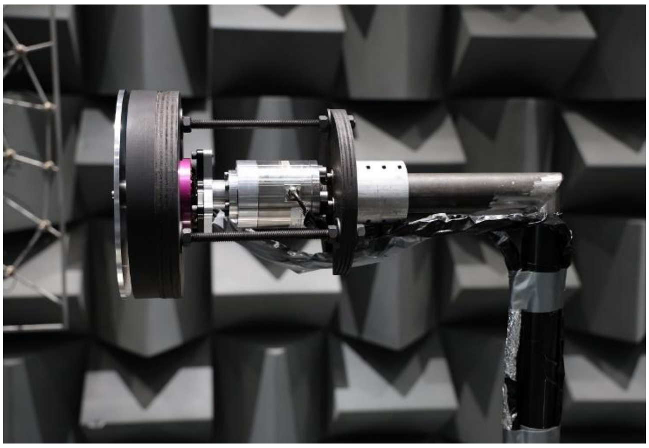

Figure 6: Picture of magnetic brake in AWT facility.

First, measured electrical power and propeller RPM for the rotor setup were collected for different wind tunnel speeds and turntable angles. Then for the selected hover conditions at a specific RPM the distance between the alu disk and magnetic plane was varied in steps, while measuring the required power, see Figure 7.

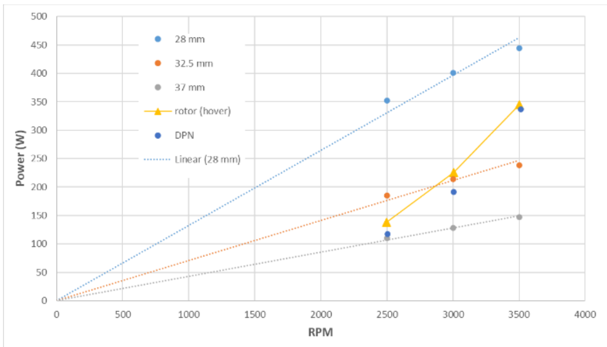


Figure 7: Electric power versus RPM for various magnetic disk distances.

The power varies linearly with RPM for the magnetic brake, but the configuration with rotor shows a typical cubic curve where matching conditions can be found.

Motor noise has been investigated by plotting narrowband spectra, e.g. see Figure 8.

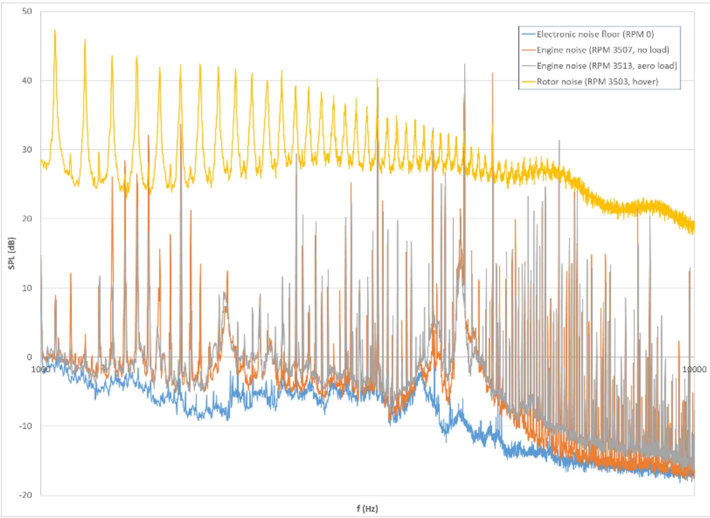


Figure 8: Motor noise spectra.

Comparison with background noise shows sufficient signal-to-noise ratio in the full range. Analysis for cases where the shaft loading is closely matching the aerodynamic loading for a rotor configuration revealed that i) the motor noise spectrum contains clusters of engine order peaks and has highest levels in the middle frequency range (here 3-5 kHz), ii) the aero load modifies the motor noise (in idling conditions) in a complex way (decreased SPL for certain low-order frequencies and increased SPL for certain high-order frequencies), iii) rotor noise is characterized by dominating tonal noise is a wide frequency range, except for some frequencies where motor noise (under aero loading) is dominating.

## 5. FLYOVER FIELD TEST OF MULTI-ROTOR UAV

### 5.1. Test and measurement setup

NLR's Drone DigiCity is an innovative test facility where drones and systems can be operated in a simulated urban environment. This 'smart city' comprises 24 shipping containers that can be configured in various ways, see Figure 9. To monitor this environment a high-tech digital infrastructure is developed with sensors and measurement devices in the city and on drones [15].


Figure 9: Picture of NLR's Drone DigiCity.

In order to generate an experimental database to be used for multi-rotor noise validation purposes, a field test campaign has been performed. A DJI Matrice M600 drone has been operated to simulate a multi-rotor UAV, see Figure 10. The drone was outfitted with an RPM sensor for each rotor, enabling the autopilot system to track and record the drone's position and orientation. Furthermore, a temperature sensor was installed on the drone to measure the local air temperature.

Figure 10: Picture of M600 drone, parked on ground.

The full test campaign considered multiple flight trajectories and 22 microphones, see Figure 11, and is elaborated in Ref. [16]. The present paper is constrained to a single free-field microphone (PCB 378A06, including a B&K windscreen) located 1.2 m above the ground, see Figure 12. Time signals were recorded with a GBM VIPER-HDR dynamic data acquisition system [19] and M+P software [20]. The microphone sensitivity at 1 kHz was calibrated and repeatedly checked with a GRAS 42AG sound calibrator. Acquisition was performed with a high-pass filter of 1.5 Hz and a sampling frequency of 65.535 kHz.

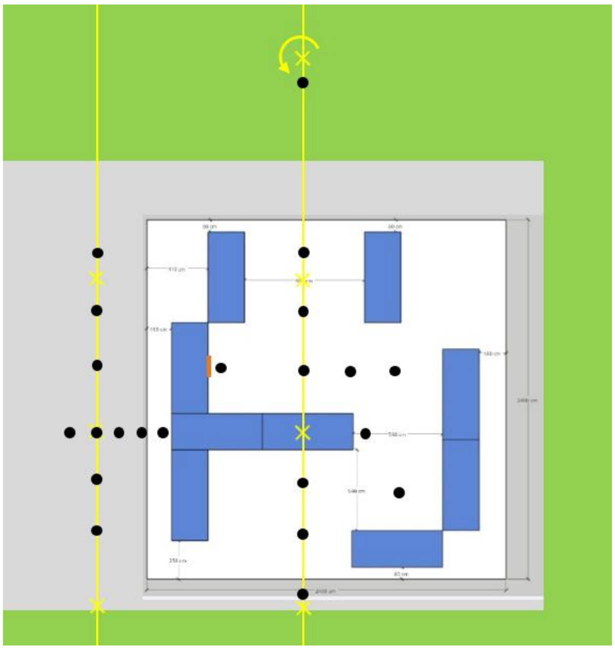

Figure 11: Top view sketch of full campaign flight paths and microphone locations [16].

Figure 12: Picture of M600 drone, hovering above free-field microphone outside of DigiCity zone.

Three flight conditions have been recorded: hover (8.5 m above microphone, 0 m/s), flyover low-speed

(8.0 m ground height, flight speed 1 m/s) and flyover high-speed (8.0 m ground height, flight speed 10 m/s). The hemispheres resulting from noise predictions have been taken as input for sound propagation modelling with geometric spreading correction and atmospheric damping correction to allow comparison with test data from the specified free-field microphone.

### 5.2. Test results and model validation

In order to compare the predictions and measurements, spectrograms have been generated. The SPL at the physical microphone location in the field is defined as monitoring point. For flyover conditions test data and predictions have been synchronized. The results are shown in Figure 13 - Figure 15, where the experimental spectrograms are in the top figure. The predicted spectrograms will be discussed in more detail while showing SPL spectra comparisons.

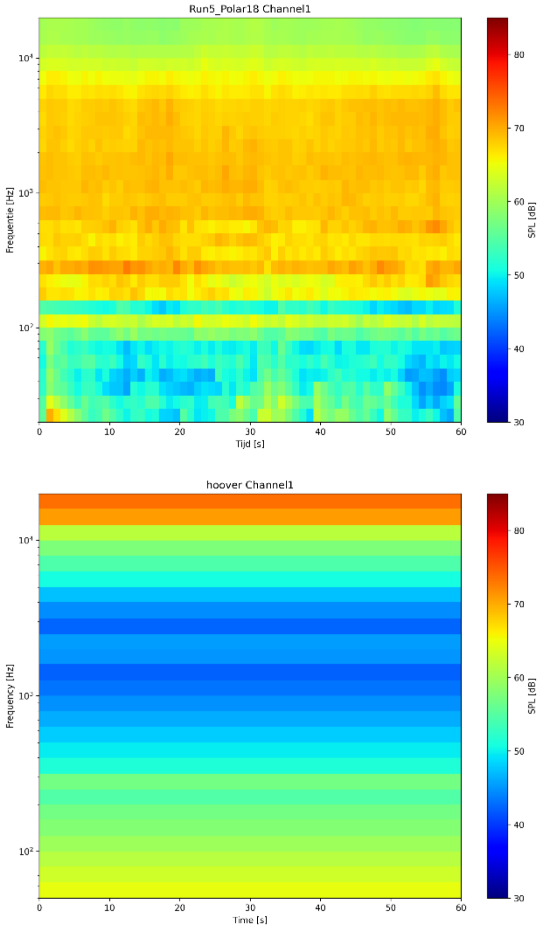


Figure 13: Validation of multi-rotor noise for hover condition. Top: spectrogram measurement, Bottom: spectrogram prediction.

For each flight condition, the experimental and predicted spectrogram have the same contour level range. The experimental spectrogram for a hover condition (Figure 13) shows significant SPL in a broad frequency range, where tonal components of the first BPFs are also visible. It is noted that wind gusts have been observed to have an effect on the spectrogram, e.g. see Figure A 1. It can be seen that the wind has two types of effect. First, it causes fluctuations in the low-frequency range, below the 1st BPF. This is pseudo-noise generated in the condenser microphone due to hydrostatic pressure fluctuations, revealing reduced effectiveness of the windscreen. Second, the wind causes delayed elevation/modulation of the high-frequency (rotor) noise levels. Investigation of this phenomenon is beyond the scope of the present paper.

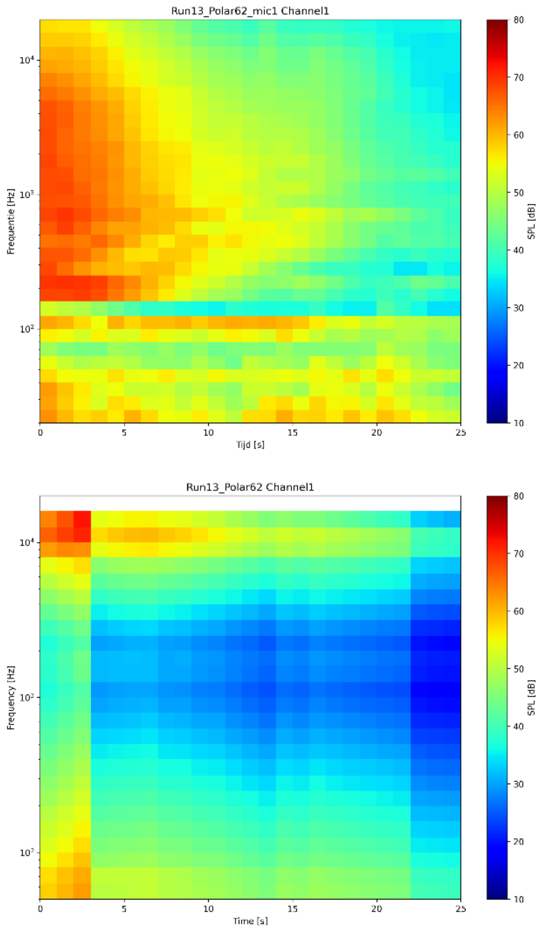


Figure 14: Validation of multi-rotor noise for low-speed flyover (1 m/s). Top: spectrogram measurement, Bottom: spectrogram prediction.

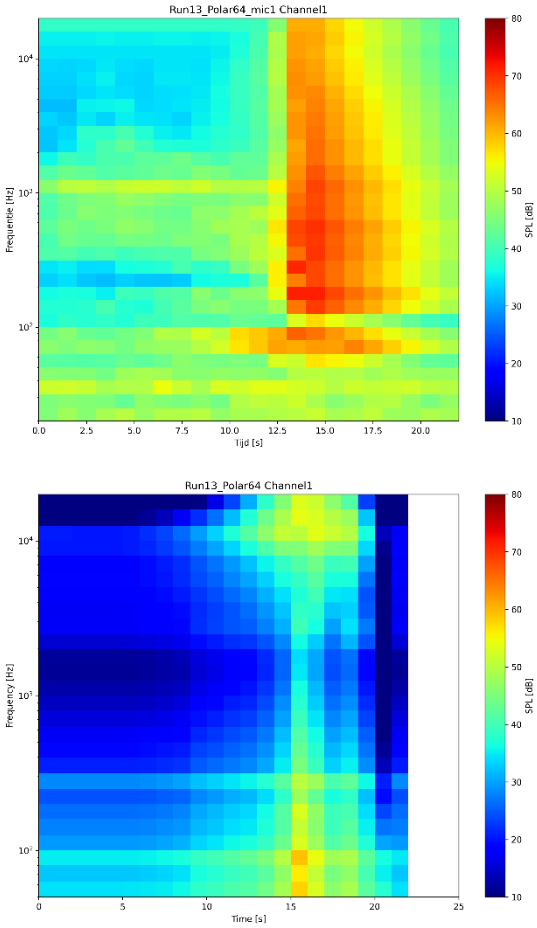


Figure 15: Validation of multi-rotor noise for high-speed flyover (10 m/s). Top: spectrogram measurement, Bottom: spectrogram prediction.

The experimental spectrograms for a flyover condition (Figure 14 - Figure 15) also show significant SPL in a broad frequency range, with visible tonal components of the first BPFs suggesting directivity effects. The flyover time just above the microphone is i) 5 s for low-speed, ii) 16-17 s for high-speed.

Noise source predictions have been performed extensively, yielding a variety of hemispheres. The predictions include rotor tonal noise (ROLLNAX) and rotor broadband noise. For the latter the BPM model is used with many parameter variations (breakdown TE sources, tripping state, blade specific boundary layer or BPM, TE geometric representation) and addition of the TI model (with variations in turbulence dissipation rate). The predicted spectrograms shown in the preceding figures are based on the classical BPM model added with TI noise. This is described in the following paragraph.

Figure 16 - Figure 18 show comparisons of the SPL spectra for each flight condition just above the microphone. All flight conditions show a similar effect. First consider the predictions with the BPM untripped Turbulent Boundary Layer TE noise source (blue curves). The spectra show rotor BPFs and rotor broadband noise in distinct frequency regions. However, a spectral comparison with experimental data (orange curves) show in general underprediction of rotor tonal- and broadband noise. The experimental results show in general relative flat spectra, where the BPFs and middle frequencies are covered by broadband noise. It is however noted that the frequency axis contains 1/3 octave bands. In an attempt to understanding improvement potential noise sources are added to the predictions. Adding both the TI noise source (turbulence dissipation rate set to relative low value of 0.01 $m^2/s^3$) and Laminar Boundary Layer Vortex Shedding and TE Bluntness Vortex Shedding sources yields improvement in, respectively, the low- and high frequency range (grey curves). However, it still does not capture the relative flat experimental SPL spectrum.

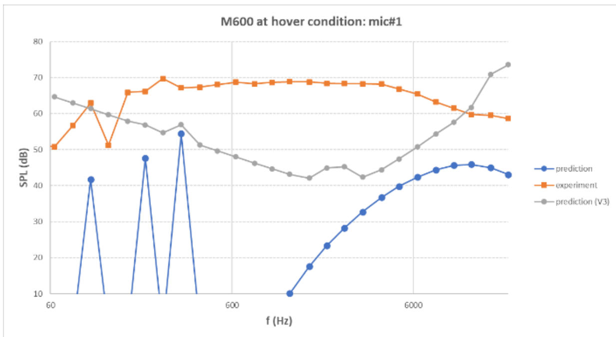


Figure 16: Comparison of noise spectrum during hover above free-field microphone.

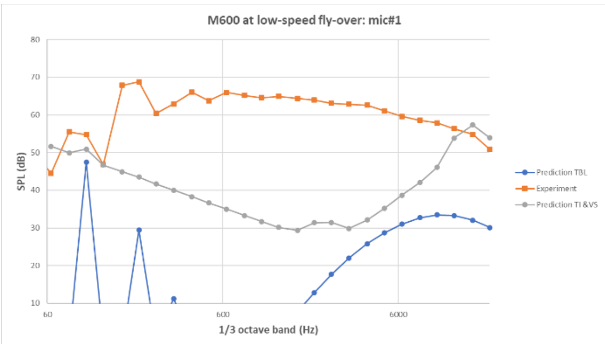


Figure 17: Comparison of noise spectrum during low-speed flyover (1 m/s) above free-field microphone.

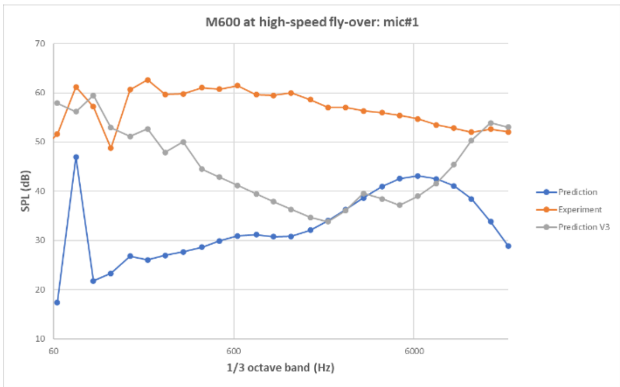


Figure 18: Comparison of noise spectrum during high-speed flyover (10 m/s) above free-field microphone.

In order to better understand the differences between predicted and measured noise spectra, a brief assessment of the multiple-rotor speed distribution has been performed. The predicted rotor speeds showed a perfectly constant RPM for hover and a typical distribution (lowest RPM for head rotors and highest RPM for aft rotors) during forward flight, see Figure A 2. However, the distribution as measured (Figure A 3) showed i) relative strong rotor variations in RPM during forward flight, ii) relative strong fluctuations in RPM during forward flight, but iii) a similar trend in reduced RPM when considering high-speed flight against hover. In addition, it can be observed that the measured RPM is overall higher than predicted.

Finally, a comparison of the measured noise spectra shows that the 2nd BPF is the dominating tone (unweighted SPL) and reduces its level from hover to high-speed flight, see Figure A 4. In addition, it can be observed that the middle/high-frequency range (from which part of it is rotor broadband noise) reduces its SPL up to approx. 10 dB from hover to high-speed flight. Although the rather flat spectra have also been observed in other publications, the order of magnitude for the SPL differences as found in the present work is significantly higher than the stated 3 dB between hover and forward flight [22].

## 6. CONCLUSIONS

1. The Pegg model is the oldest considered semi-empirical rotor broadband noise model. An isolated rotor WT test showed that Pegg's model significantly underpredicts the peak frequency and overpredicts the peak level. This is in line with external observations [11] and might be related to its helicopter based application range.
2. The GL model is the most recent considered semi-empirical rotor broadband noise model. An isolated rotor WT test showed large deviations with the predicted spectra. Analysis suggest that the GL model is not suited for the "flying hemisphere" approach, as it does not have a far-field solution.
3. The increasingly applied BPM model for rotor broadband noise predictions was used for comparison with results of an isolated rotor in a wind tunnel. The BPM model overpredicted the peak frequency and underpredicted the peak level. Simulating a tripped condition showed improvement in peak frequency.
4. In order to generate an experimental database to be used for multi-rotor noise validation purposes, a field test campaign has been performed. The predicted spectrograms of hover and flyover events show in general an underprediction for all noise components. This holds for rotor tonal noise (rotating lifting line method, BPF 1-3) and rotor broadband noise (BPM model, underprediction of peak SPL and overprediction of peak frequency).
5. A comparison of the 6-rotor speed distribution between prediction and measurements revealed an overall underprediction in averaged RPM. Although the relative high fluctuations in RPM during flyover complicate the assessment, these results suggest that at least part of the found SPL underprediction can be explained by differences in RPM. The measured relative high fluctuations in RPM also suggest an additional noise source yielding underprediction. The root cause is currently hypothesized in too optimistic blade steady load aerodynamic coefficients used as input to FLIGHTLAB.
6. The BPM model does not capture non-deterministic narrowband noise, although observed in field test data of a drone flyover event. However, it is shown that the low-frequency range predictions can be improved by including atmospheric turbulence ingestion (TI model). The effect of turbulent wake ingestion is not considered.
7. Dedicated laboratory tests with a specially designed magnetic brake (i.e. without rotor blades) have been performed to assess motor noise. Analysis for cases where the shaft loading is closely matching the aerodynamic loading for a rotor configuration revealed that i) the motor noise

spectrum contains clusters of engine order peaks and has highest levels in the middle frequency range (here 3-5 kHz), ii) the aero load modifies the motor noise (in idling conditions) in a complex way (decreased SPL for certain low-order frequencies and increased SPL for certain high-order frequencies), iii) rotor noise is characterized by dominating tonal noise in a wide frequency range, except for some frequencies where motor noise (under aero loading) is dominating.

8. Dedicated WT tests showed that the middle frequency range is characterized by tonal noise, although this range is not predicted by the considered semi-empirical prediction models. Future research should be conducted to reveal the relative contribution of electric motor and deterministic rotor noise sources in this frequency range. The measured noise spectra during flyover tests are relatively flat in 1/3 octave band resolution. Narrowband analysis could reveal the contribution of tonal noise components.

9. Contrary to UAM, UAV systems are abundantly available and their noise sources could be obtained via field tests. Empirical free-field noise models, which do not suffer from high uncertainty in the mid/high frequency range, could then be used in predicting noise maps of urban environment or vertiports [22,23].

10. The found results for the multi-copter field test suggest that noise emission during hover and forward flight can be significant, with level differences up to 10 dB in the middle frequency range, so that hover measurements (e.g. in the laboratory) may not be used as first proxy emission characteristics of high-speed forward flight).

Author contact:

remco.habing@nlr.nl

## 7. APPENDIX

The appendix contains additional figures, that are cited in the body text of this paper.

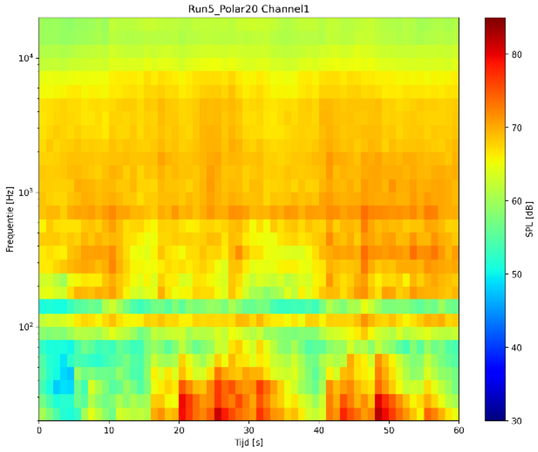


Figure A 1: Effect of wind gusts on spectrogram measurement for hover condition.

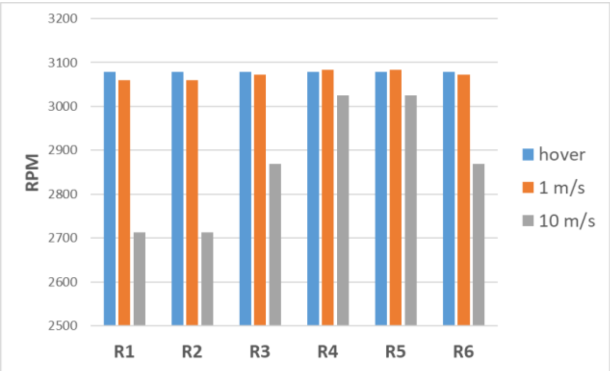


Figure A 2: Predicted rotor speeds for tested conditions.

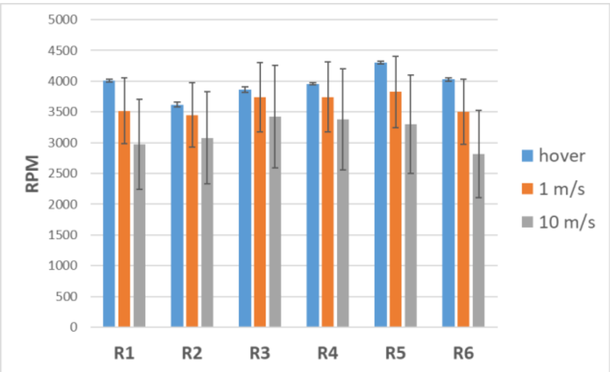


Figure A 3: Measured rotor speeds for tested conditions.

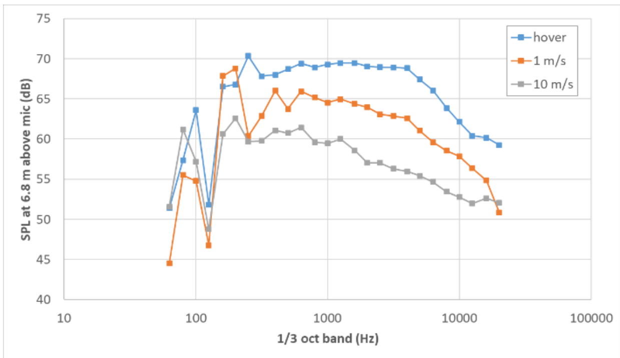


Figure A 4: Comparison of measured noise spectra for tested conditions.

## 8. ACKNOWLEDGMENTS

Part of this research is conducted within the research and innovation programme Luchtvaart in Transitie, which is co-funded by the Netherlands National Growth Fund.

## 9. REFERENCES

1. Greenwood, E., Brentner, K. S., Rau, R. F., & Ted Gan, Z. F. (2022). Challenges and opportunities for low noise electric aircraft. International Journal of Aeroacoustics, 21(5-7), 315-381.
2. Brooks, T. F., & Schlinker, R. H. (1983). Progress in rotor broadband noise research. Vertica, 7(4), 287-307.
3. Habing, R. et. al, A Noise Prediction Tool for IAM and AAM in Urban Environments, paper 049, ERF 2024.
4. Drela, M., XFOIL: An analysis and design system for low Reynolds number airfoils, Low Reynolds number aerodynamics, Springer-Verlag Lec. Notes in Eng. 54, 1989.
5. FLIGHTLAB. (n.d.). Home. Retrieved January 17, 2024, from https://www.flightlab.com/
6. Brouwer, H. H. (1992). On the use of the method of matched asymptotic expansions in propeller aerodynamics and acoustics. Journal of Fluid Mechanics, 242, 117-143.
7. Brouwer, H. H., The Scattering of Open Rotor Tones by a Cylindrical Fuselage and its Boundary Layer. AIAA Paper 2016-2741, 2016.
8. Brooks, T. F., Pope, D. S., & Marcolini, M. A. (1989). Airfoil self-noise and prediction (No. L-16528).
9. Van der Meulen, M.P., Knepper, K.M. & Brouwer, H.H., Translating acoustic wind tunnel data to full scale aircraft noise; Incorporation of aircraft noise models in ENOISE, NLR-CR-2016-374, 2019.
10. Pegg, J., A summary and evaluation of semi-empirical methods for the prediction of helicopter rotor noise, NASA TM 80200, 1979.
11. Gill H. & Lee S., Development of new empirical rotor broadband noise prediction models for urban air mobility applications, AIAA Scitech 2024-2473, 2024.
12. Buck S., Oerlemans S. and Scott P., Experimental Validation of a Wind Turbine Turbulent Inflow Noise Prediction Code, AIAA J. Vol. 56, No. 4, April 2018.
13. Kadaster. (n.d.). 3D Geluid., from https://3dgeluid.kadaster.nl/3dgeluid/
14. Kephalopoulos, S., Paviotti, M., & Anfosso-Lédée, F. (2012). Common noise assessment methods in Europe (CNOSSOS-EU). Common noise assessment methods in Europe (CNOSSOS-EU), 180-p.
15. NLR Drone DigiCity, https://www.nlr.org/newsroom/nieuws/experimenting-in-a-simulated-urban-area-with-drone-digicity/
16. Knepper, K. et al., Experimental database for AAM noise assessment in urban environment, paper 518, ERF 2025.
17. Li S. and Lee S., Prediction of Urban Air Mobility Multirotor VTOL Broadband Noise Using UCD-QuietFly, JHS 66, 2021.
18. Bertagnolio F, et. al, Wind Turbine Noise Code Benchmark: A Comparison and Verification Exercise, 10th Int. Conf. Wind Turbine Noise, June 2023.
19. H. Holthusen and H. Smit, “A new data-acquisition system for microphone array measurements in wind tunnels”, AIAA paper 2001-2169, 2001
20. M+P. Home, Retrieved February 17, 2025, from https://mpihome.com/en/
21. Elshof, T., Validation of an engineering tool for broadband noise prediction of UAV and UAM configurations in hover conditions, MSc thesis, University of Twente, 2025.

22. Schäffer, B. et. al, Drone Noise Emission Characteristics and Noise Effects on Humans—A Systematic Review, Int. J. Environ. Res. Publ. Health 18, 2021.
23. Granberg, T.A., D4.3 Noise and visual pollution tools and concepts, AiRMOUR project, 2023.